# TEMPERING OF STEEL DURING LASER TREATMENT

Hegge, H.J.; Beurs, H. de; Noordhuis, J.; De Hosson, J.T.M.

*Published in:*
Metallurgical transactions a-Physical metallurgy and materials science

*DOI:*
10.1007/BF02656583



*Publication date:*
1990

# Tempering of Steel during Laser Treatment

H.J. HEGGE, H. De BEURS, J. NOORDHUIS, and J.Th.M. De HOSSON

This study concentrates on the annealing effects of a laser-treated area by a successive laser pass in a plain carbon, a chromium, and a tungsten steel. Transmission electron microscopy (TEM), optical microscopy (OM), and wear and hardness measurements revealed substantial effects on the properties and microstructure of the plain carbon and tungsten steel which have a partly martensitic cellular structure after the first laser treatment. Close to the melt zone, martensite was again formed, whereas further away, nucleation of carbides was observed. The hardness increased in the former area and decreased in the latter. An analytical model sustained that the softening is due to carbon diffusion and martensite tempering. The softer zone in the tungsten steel exhibited a decrease of wear rate relative to the not-annealed zone in contrast to the plain carbon steel. Besides some diffusion, no annealing effects were found in the chromium steel which possessed an austenitic cellular structure after the first laser treatment.

## I. INTRODUCTION

TEMPERING of steel is a common practice and already has been studied for more than a century. Usually steel is heat-treated after quenching to improve its mechanical properties. Laser treatment is a comparable process. During the passage of a laser beam after possible melting and resolidification, the heat is conducted away to the substrate, and high cooling rates are attained. Several authors have investigated laser treatments on different types of steel.[1–13] The hardness and wear resistance is improved with respect to conventionally quenched steel.[4,7,9–12]

When a laser is used in practical applications, it is usually necessary to scan the complete surface, *i.e.*, the laser beam passes a previous track a small distance away. This area is exposed to a thermal cycle and is tempered during a short time (Figure 1).

Some authors have reported on laser-treated material tempered in a rather conventional way.[1,8] A fine distribution of carbides was found. Austenite was discovered to be rather stable. In a laser-tempered pass, a lower hardness has been reported together with a tensile stress compared with the higher hardness and the compressive stress in the not-tempered pass.[13] An AISI 1045 steel showed a decreasing hardness and higher sensitivity to etching in the laser-tempered area.[5] Nonetheless, the picture of laser tempering and its effect on the mechanical properties of a laser-treated surface is rather incomplete, and an appropriate explanation is not available.

In this study, attention is paid to these subjects dealing with three different types of steel. After laser treatment, one type shows an austenitic, another a martensitic, and a third a mixed structure of δ-ferrite, austenite, and martensite. The layers are analyzed and mechanically tested. A simple analytical model is presented to reveal the reason why the tempering effect is sometimes quite large despite the short duration time of the laser passage.

H.J. HEGGE and H. De BEURS, formerly Graduate Students, Department of Applied Physics, Materials Science Centre, University of Groningen, are with Shell Corporation, The Hague, and Philips Corporation, Drachten, respectively. J. NOORDHUIS, Graduate Student, and J.Th.M. De HOSSON, Professor of Applied Physics, are with the Department of Applied Physics, Materials Science Centre, University of Groningen, Nijenborgh 18, 9747 AG Groningen, The Netherlands.

Manuscript submitted March 7, 1989.

## II. EXPERIMENT

The chemical compositions of the steels used are listed in Table I.

The specimens were ground and grit-blasted to get a rough surface which absorbed well the laser light used (size: 38-mm diameter, 5-mm thickness). After grit blasting, the samples were ultrasonically cleaned and annealed during 90 minutes at 920 K. The hemispherical absorption for the wavelength used (10.6 μm) was more than 30 pct at room temperature.

The specimens were mounted on a numerically controlled *X-Y* table and irradiated by a 1.5 kW Spectra Physics 820 $CO_2$ laser. The Gaussian beam (19-mm diameter) is deflected by a Mo mirror and focused by a ZnSe lens before it impinges upon the surface. At the surface, the power of the beam was 1300 W. The focus point of the lens lay 5.0 mm above the surface (focal length of the lens: 127.0 mm, shielding gas: Argon). The laser scanned the surface with a velocity between 1 and 40 cm/s. The delay time between two passes was 1 minute to cool the samples down to room temperature again. The overlap of the melted tracks was about 1/4 of the width (also see Table II). After the laser treatment, cross-sectional samples were prepared for hardness measurement, optical microscopy (OM), and scanning electron microscopy (SEM). Etching fluid Villela reagent was used which clearly revealed the annealed areas where carbides are grown in Fe-C and Fe-W. Vickers and Knoop hardness measurements with weights of 0.5 and 1 N were made on the cross sections. To get the reliable results, microscopy indentations were placed in a row parallel to the surface and about 1.5 times the length of the diagonal below it. Transmission electron microscopy (TEM) samples were prepared by spark cutting (<0.2-mm thickness) parallel and just below the surface and thinning electrochemically until an electron transparent area was attained. Sometimes ion milling was used to get a larger transparent area.

The macroscopic wear performance of laser-melted steel is tested on a pin-on-disk wear tester.[17] Before wearing,

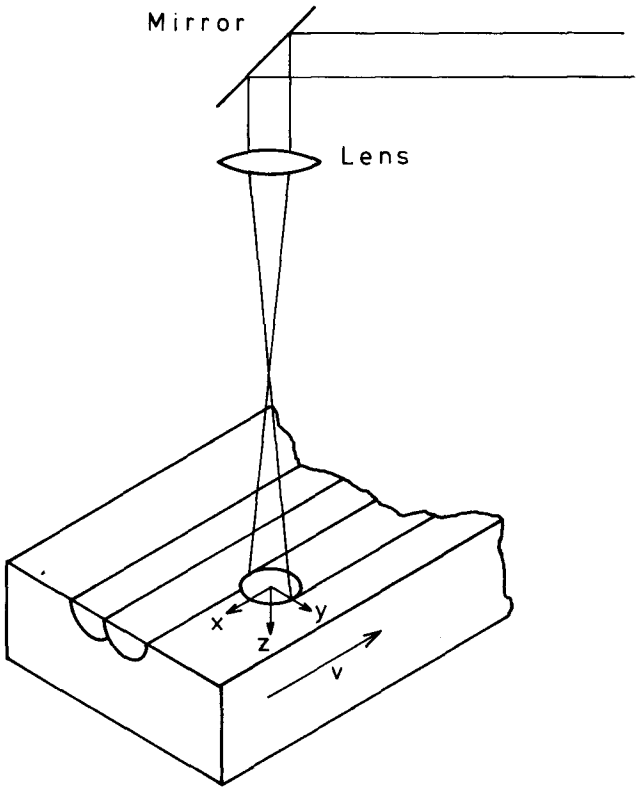


Fig. 1—Laser beam scanning the surface.

the hardened surfaces are slightly polished with SiC paper and diamond paste. A ruby crystal ball with a 5-mm diameter is pressed upon a rotating sample. The ball does not show any significant damage during the experiments. Before each test, the ball is rotated or replaced in order to have a well-defined starting condition. For all experiments, a constant speed of 0.5 cm/s and a constant load of 2.3 N have been chosen. According to Hertzian stress analysis, it can be shown that in the present situation, no plastic yielding due to the ball pressure occurs. The effect of humidity is reduced by supplying absolute ethanol and working in an atmosphere of 85 pct Ar and 15 pct $H_2$. Locally, on the wear track, the amount of wear is determined with an interference microscope. Figure 2 shows the wear tracks of different materials around the heat-affected zone. The micrographs reveal local and periodic oxidation of the wear tracks of Fe-W and Fe-C steels. It is caused by a change in composition due to the growth of carbides.

In order to investigate the effect of overlap, a large overlap of the tracks is chosen; hence, the laser-melt treatments are carried out with a lower speed than has been used for the other experiments. The parameters used are focus: +5 mm, distance between passes: 0.6 or 1 mm, and scan velocity: 1 cm/s.

**Table II. Distance between Laser Tracks**

| | Hardness Measurements (1 cm/s) [mm] | Wear Experiment [mm] |
|---|---|---|
| Fe-C | 0.6 | 1.0 |
| Fe-Cr | 0.6 | 0.6 |
| Fe-W | 0.6 | 0.6 |

## III. RESULTS

### A. *Fe-C*

The effect of tempering on the hardness is pronounced (Figure 3). The softened zone ranges up to a width of 500 $\mu$m at the surface at a laser scanning velocity of 1 cm/s and a focus of 5 mm. The structure of the tempered zone is shown in Figure 4. The onset of the tempered zone is concluded from the etched structure, and the end of the tempered zone is determined by hardness measurements. The width of the total heat-affected zone at the surface for various laser scan velocities together with the width of the softened zone as determined by hardness measurements are depicted in Figure 5. In the heat-affected primary melt zone, two areas can be distinguished. First, the zone where the peak temperature exceeds the $A_1$ temperature and, during quenching, martensite might be formed. Second, if the peak temperature is below the $A_1$ temperature, only softening occurs, and carbide growth takes place (Figure 6).

The wear performance across the heat-affected zone is measured for 2000 and 8000 turns. This is represented in Figure 7 together with the hardness profile. In this figure, the $X$-axis is normalized where 1 stands for the onset of the heat-affected primary melt zone and 0 is the start of the next cycle. At the onset of the tempered zone, corrosion occurs and the wear volume is not measured. The constant wear profile in the case of 2000 turns is remarkable. At 8000 turns, an increase in the wear rate is found in the softer area.

### B. *Fe-Cr Steel*

During laser melting, no change in hardness is found in the heat-affected primary melt zones (Figure 8). Also, the wear volume across the overlapping zone is found to be constant (Figure 9). In the original structure of laser melted Fe-Cr consisting of austenite cells surrounded by $M_3C$ carbides (Figure 10), neither carbide growth nor transformation of austenite into martensite or ferrite has been found. Probably there is some local remelting of the eutectic cell boundary, as shown in Figure 11, but then it also resolidifies into $M_3C$ carbides. Electron dispersive spectrometry measurements revealed that very little Cr was diffused away from the cell boundaries.

**Table I. Chemical Compositions of the Materials Used (Weight Percent)**

| Name | C | Si | Mn | Cr | V | W | Fe |
|---|---|---|---|---|---|---|---|
| Fe-0.6 | 0.65 | 0.09 | 0.99 | 0.24 | — | — | bal. |
| Fe-W | 0.75 | — | — | 4.25 | 1.05 | 18.0 | bal. |
| Fe-Cr | 2.05 | — | — | 11.5 | — | 0.7 | bal. |

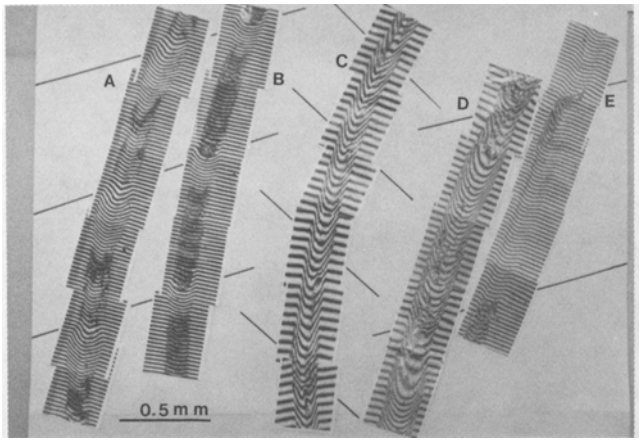


Fig. 2—Several wear tracks viewed by interference microscopy: (*a*) Fe-W 8000 turns, (*b*) Fe-W 10,000 turns, (*c*) Fe-Cr 8000 turns, (*d*) Fe-C 8000 turns, and (*e*) Fe-C 2000 turns.

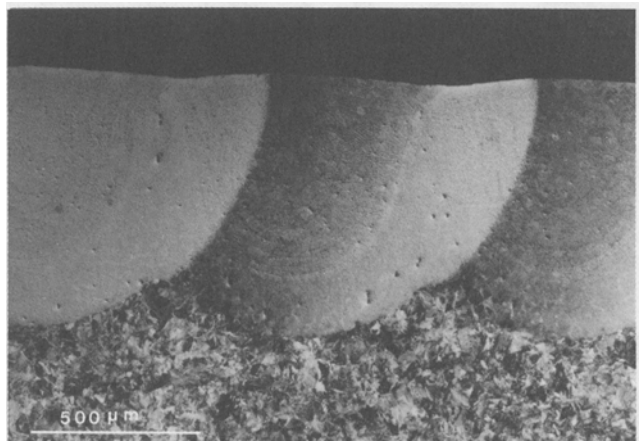


Fig. 4—Cross section of laser tracks in Fe-C (scan velocity: 6 cm/s).

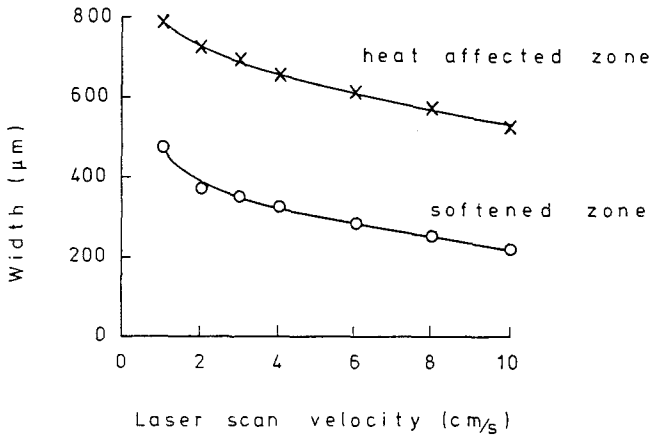


Fig. 5—Width of the heat-affected, not-melted zone and width of the softened area *vs* laser scanning velocity.

## C. *Fe-W Steel*

Overlapping of laser passes does not significantly increase the hardness but improves the wear resistance of Fe-W steel. The microstructure of laser-melted Fe-W steel has a cellular solidified structure with cells consisting of δ-ferrite embedded in martensite and retained austenite which are again surrounded by $M_6C$ carbides (Figure 12). During tempering, some processes can occur due to the heat cycle of the new adjacent track. At high temperatures, segregated carbides can dissolve and δ-ferrite can transform into austenite, eventually resulting in a larger amount of martensite after quenching. In zones with a lower peak temperature, carbides can grow (Figure 13) and the δ-ferrite might grow by transformation of austenite into ferrite. Transmission electron microscopy observations reveal carbides which have grown from 25 to 200 nm in a zone of 250 µm at the surface.

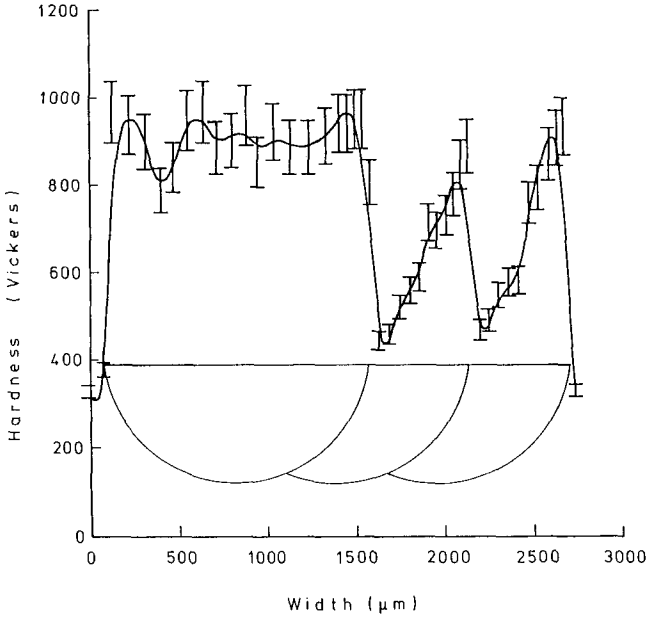


Fig. 3—Hardness profile Fe-C with a sketch of the zones heated to temperatures above which austenite forms overlapping laser passes (scan velocity: 1 cm/s).

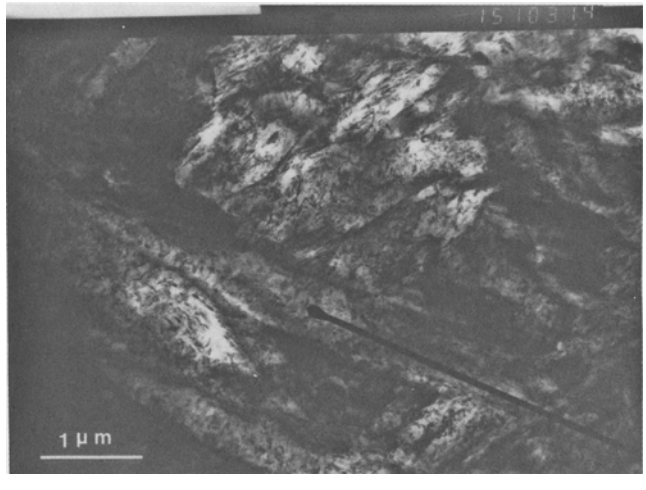


Fig. 6—Carbides in the tempered zone in Fe-C.

Laser tracks are made near each other under the same conditions as above for Fe-Cr steel. In Figure 14, the

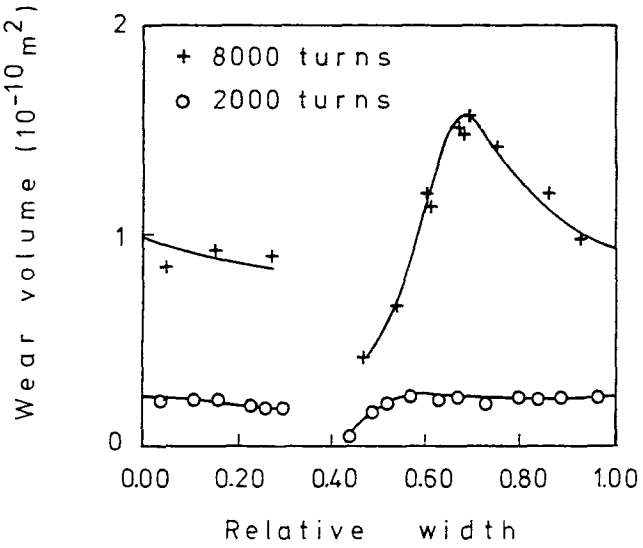


Fig. 7—Wear profile of Fe-C (scan velocity: 1 cm/s). 0 = boundary of melt zone and 1 = boundary of previous melt zone.

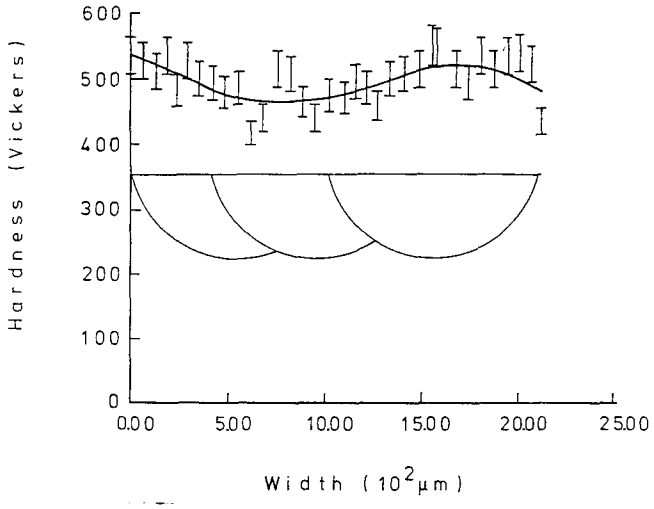


Fig. 8—Hardness profile of Fe-Cr with a sketch of the melted zones of overlapping laser passes (scan velocity: 1 cm/s).

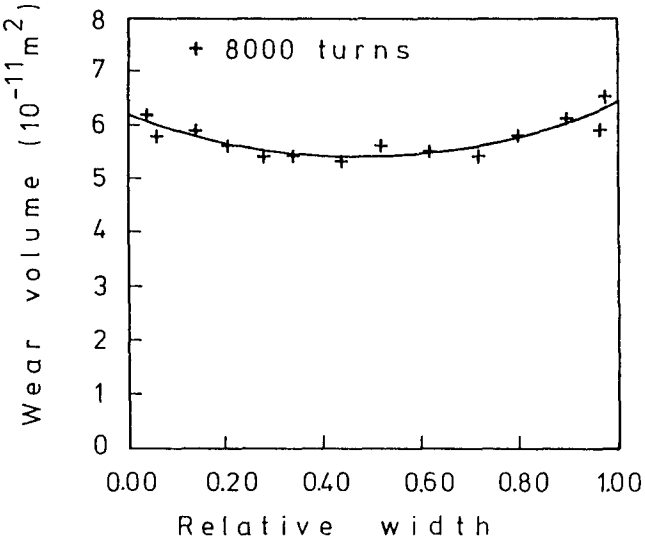


Fig. 9—Wear profile of Fe-Cr (scan velocity: 1 cm/s). 0 = boundary of melt zone and 1 = boundary of previous melt zone.

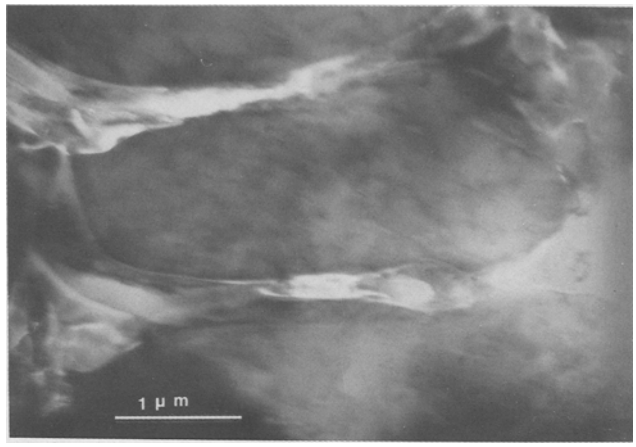


(*a*)

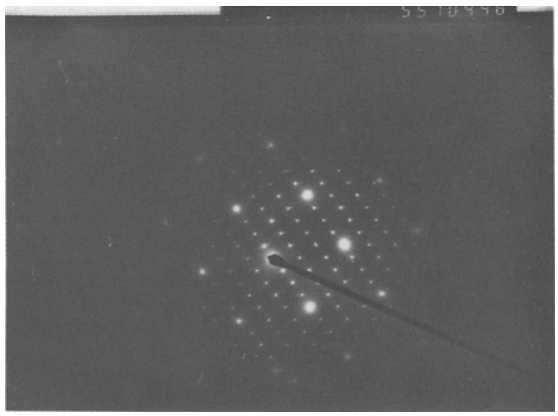

(*b*)

Fig. 10—TEM photographs of Fe-Cr (solidification structure): (*a*) bright field and (*b*) diffraction pattern.

hardness profile of only laser-melted Fe-W steel is depicted together with a local enlargement in the overlap area. To increase the lateral resolution, these measurements are done with a Knoop indenter. In the first 100 $\mu$m after the melt zone, an increase in hardness is found. A sudden decrease in hardness is found at the point where light microscopy shows growth of carbides. The hardness decreases with 200 HK after which it finally reaches the value of the only laser-melted material.

In wear experiments, the influence of carbide growth is very significant. In this zone, a reduction in wear with a factor of 4 is found in the wear rate, as shown in Figure 15.

## IV. THEORY

An analytical model[7] was applied to simulate the thermal cycle and to check in this way whether the changes can be explained by ordinary tempering mechanisms, such as diffusion of carbon and growth of carbides.

These phenomena depend on the total number of diffusive jumps during a treatment. It can be measured by the so-called kinetic strength ($I$) which is the total time

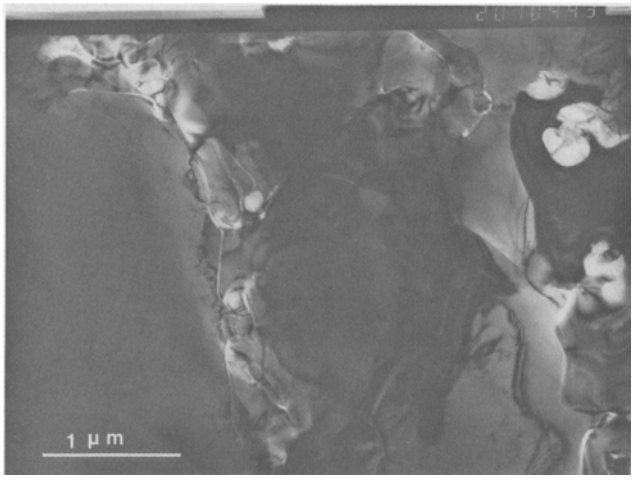


(*a*)

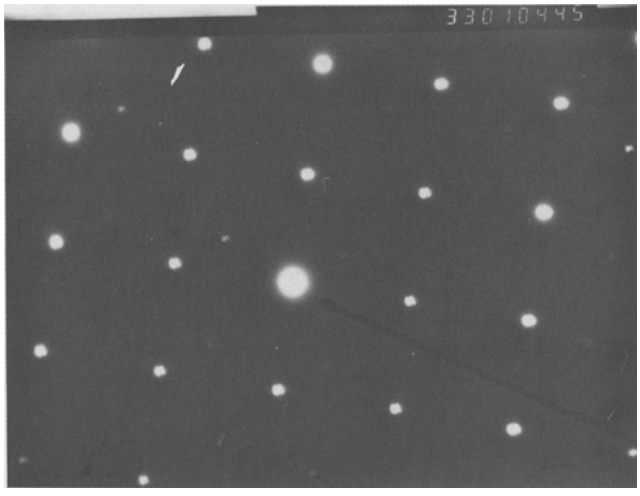

(*b*)

Fig. 11—TEM photographs of Fe-Cr (molten and resolidified cell walls): (*a*) dark field and (*b*) diffraction pattern.

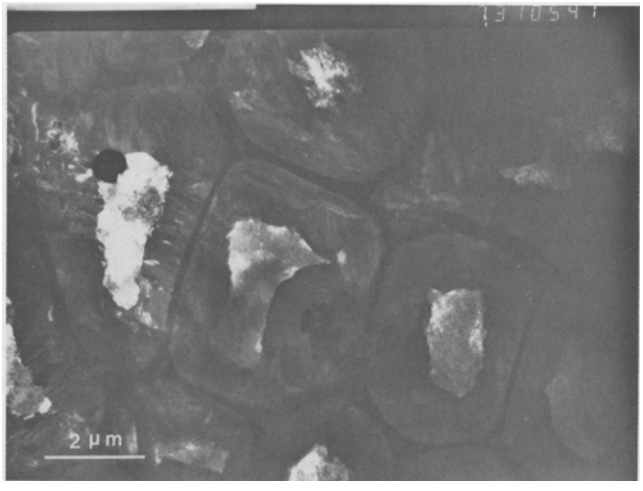


Fig. 12—TEM dark-field photograph of the δ-ferrite zone in Fe-W.

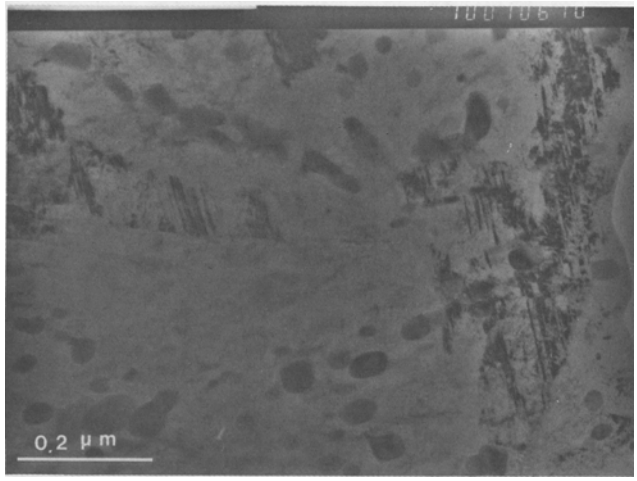


Fig. 13—Carbides in the tempered zone in Fe-W.

for the heat cycle modified by an Arrhenius factor to account for the temperature influence.

$$I(t) = \int_0^t e^{-[Q/RT(t')]}\, dt' \qquad [1]$$

where $Q$ represents the activation energy, R the gas constant, $T$ the temperature, and $t$ the time.

With the kinetic strength, some important parameters for tempering can be calculated. The total number of nuclei formed is given by

$$N(t) = \nu C_0 \int_0^t e^{-[Q/RT(t')]}\, dt' \qquad [2]$$

where $\nu$ is the jump frequency and $C_0$ represents the possible nucleation sites. (One integrates over the time during which such a temperature is reached such that nucleation can take place.) The activation energy ($Q$) for this process is

$$Q = Q_m + \frac{16\pi\gamma^3}{3(G_v - G_s)^2} \qquad [3]$$

where $Q_m$ represents the activation energy for atomic migration, $\gamma$ the interfacial energy between nucleus and matrix, $G_v$ the Gibbs free energy of formation, and $G_s$ the strain energy due to precipitation. The diffusion distance is given by

$$x = \sqrt{D_0 I} \qquad [4]$$

where $x$ represents the diffusion distance and $D_0$ the pre-exponential of the diffusion constant.

For the temperature field, a line source was taken, because at the high scanning velocities used in this study, the circular beam can be treated as a line. The source was positioned at a distance $z_0$ above the surface to avoid infinitely high temperatures at the surface.

$$T - T_0 = \frac{A\, q/\sigma}{2\pi\lambda(t(t + t_0))^{1/2}} \cdot \exp\left(\frac{-1}{4a}\left(\frac{(z + z_0)^2}{t} + \frac{y^2}{t + t_0}\right)\right) \qquad [5]$$

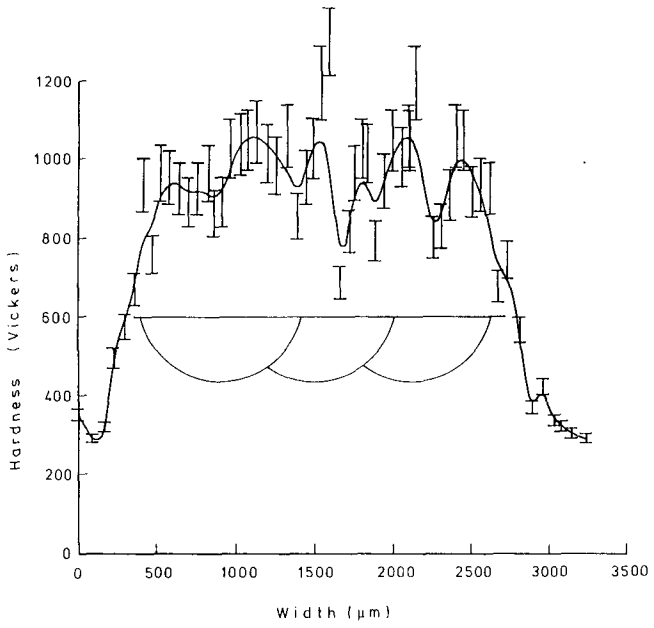


(a)

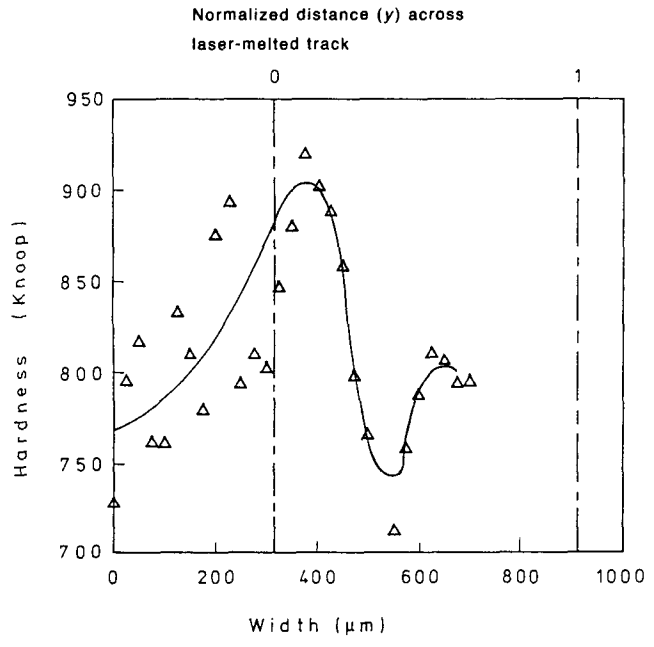


(b)

Fig. 14—Hardness profile of Fe-W (scan velocity: 1 cm/s): (*a*) overall view with a sketch of the melted zones of overlapping laser passes and (*b*) Knoop measurements of a part (0 = boundary of melt zone and 1 = boundary of previous melt zone).

where $T_0$ represents the ambient temperature, $\lambda$ the thermal conductivity, $A$ the absorption, $q$ the light intensity, $\sigma$ the laser scan velocity, $a$ the thermal diffusivity, $z$ the depth, and $y$ the width with

$$t_0 = \frac{r_b^2}{4a} \qquad [6]$$

$r_b$ being the beam radius.

If the activation energy is independent of the temperature, as is the case for diffusion, $I$ can be approximated in a laser treatment by[7]

$$I = \sqrt{\frac{2\pi R T_p}{Q}} \frac{A\,q/\sigma}{2\pi e(T_p - T_0)} e^{-(Q/RT_p)} \qquad [7]$$

$T_p$ represents the peak temperature during laser treatment. The peak temperature is obtained for $t \gg (r_b^2/4a)$ or $z^2 + y^2 \gg r_b^2\,2$; *i.e.*, far away from the laser beam, as in our case,

$$T_p = T_0 + \frac{2A\,q/\sigma}{e\pi\rho c((z + z_0)^2 + y^2)} \qquad [8]$$

where $\rho$ is the density and $c$ the heat capacity. The value of $z_0$ depends on the area one is interested in. In our case, this area is relatively far away from the laser beam, and $z_0$ is best approximated by

$$z_0^2 = \sqrt{\frac{\pi a r_b}{\sigma}} \frac{r_b}{e} \qquad [9]$$

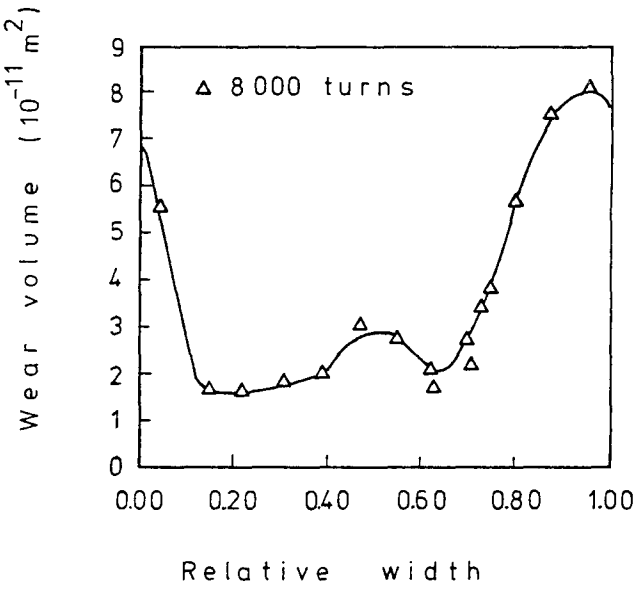


Fig. 15—Wear profile of Fe-W (scan velocity: 1 cm/s). 0 = boundary of melt zone and 1 = boundary of previous melt zone.

## V. DISCUSSION

During a heat treatment after quenching, metastable phases are usually annealed to more stable phases. In this study, the tempering cycle itself, although intense, has a very short duration. Especially on Fe-C, rather large effects on the wear rate and the hardness have been measured. The cooling rate during the tempering cycle is high enough to re-create martensite if the austenitizing temperature is reached, as can be seen near the molten region in Fe-C and Fe-W.[7,9]

The rather dramatic softening of the rest of the martensite in the heat-affected zone is less expected. The microstructure of the "as-treated" Fe-C is a martensitic lath structure with a fine prior austenite cell size (1 $\mu$m).

The structure of Fe-W also has a cellular-dendritic size in the order of 1 $\mu$m. The high hardness after the first

laser treatment is due partly to the fine cells separated by hard thick walls and partly to the martensitic structure.[12]

The softening seems to be caused mainly by the tempering of the martensite. Because the cells retain their austenitic structure in Fe-Cr, the only contribution to a change of mechanical properties would come from changes in the cell walls. Although some diffusion could be detected, it did not give rise to detectable fluctuations of the hardness.

To answer the question whether or not there is enough time to get reasonable diffusion, the kinetic strength was calculated at the surface for Fe-C with $A = 0.25$, $q = 1300$ W, and $v = 4$ cm/s (Figure 16). At the place in the experiments where annealing was scarce, a diffusion distance of 1.1 $\mu$m was found, which is of the same order of magnitude as the cell size. For other velocities, this kinetic strength was used to calculate the edge of the annealing zone, which agreed well with the experiments. In Figure 17, the annealed zone width at the surface relative to the molten and the only austenitized zone is presented. In this comparison, the austenitizing instead of the melting boundary was used, because the latter is both conduction- and convection-shaped. At the austenitizing boundary, these effects have been averaged out. The calculations were made for the range of velocities where no key-hole effect was present, because in that case, the analytical model is not applicable anymore. At high velocities (above 15 cm/s), the condition that at the peak temperature $t \gg t_0$ does not hold anymore.

Because of the low solubility of carbon, small carbides are precipitated. Apart from the diffusion, there should also be enough time for nucleation. During tempering of martensite, $\varepsilon$-carbides (at lower temperatures during the heating) and cementite (at higher temperatures) are formed.[18] Because no evidence was found of $\varepsilon$-carbides and because the heating up is very fast and during cooling cementite is first formed, the total number of cementite nuclei/$\mu$m$^3$ near the surface was computed for $v = 4$ cm/s. For the activation energy for atomic migration, the diffusion activation energy was used. The activation energy for cementite nucleation was found by subtracting the linear extrapolation from $C = 3.1$ at. pct ($\alpha$) to $C = 25$ at. pct ($Fe_3C$) of the Gibbs free energy of ferrite in which all the carbon is dissolved. Strain energy effects were neglected in this approximation. The equation of the Gibbs free energy is taken from Reference 19. In the literature, strongly different values for the interface energy between cementite and ferrite are given, *e.g.*, 0.7 J/m$^2$[20] and 1.2 J/m$^2$.[21] These values are given for large carbides with incoherent or semicoherent interfaces. However, here we are interested in the nucleation stage, during which the interface is presumably almost coherent, which is indicated by the special lattice relationship between both phases.[18] Therefore, the activation energy for cementite growth at 300 °C of 203 kJ/mol was used[22] to calculate an interface energy of 0.35 J/m$^2$. Using these values, the number of nuclei formed during a laser treatment was calculated as a function of the width (Figure 18). At widths larger than $y = 1.7$, the temperature does not reach the austenite temperature anymore and only tempering will take place. At $y = 1.8$ at the maximum, 1400 nuclei/$\mu$m$^3$ are formed after which this number decreases rapidly to less than 1/$\mu$m$^3$ at $y = 3$. This agreed remarkably well with our findings. The diffusion distance in the Fe-Cr steel

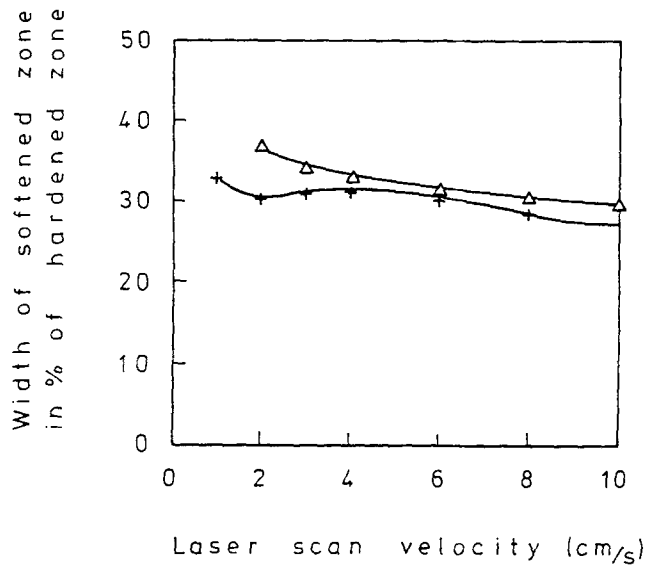


Fig. 17—Size of the softened zone (Fe-C): + = measured and Δ = calculated.

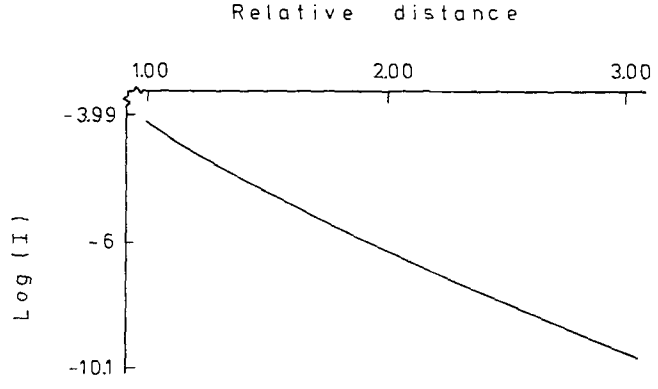


Fig. 16—Kinetic strength *vs* distance to center of the laser pass (0 = middle of melt zone and 1 = boundary of melt zone).

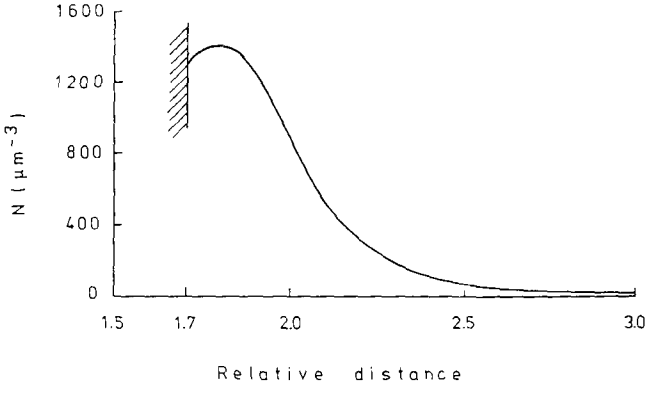


Fig. 18—Number of $Fe_3C$ nuclei *vs* distance to the center of the laser pass (0 = middle of melt zone and 1 = boundary of melt zone).

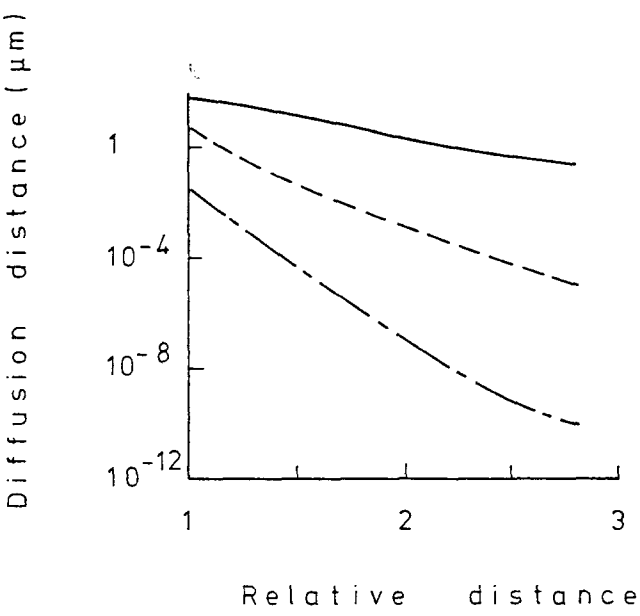


Fig. 19—Diffusion distance of carbon in ferrite (——), carbon in austenite (– – – – –), and chromium in austenite (— — — — — —) *vs* relative distance to the center of the laser pass (0 = middle of melt zone and 1 = boundary of melt zone).

was also calculated for both carbon and chromium at the surface (Figure 19) with $q$ = 1300 W, $A$ = 0.25, and $v$ = 4 cm/s. The distance of chromium diffusion, especially, was almost neglectable. If the material is austenitic (Fe-Cr), no carbides are formed in the cell interior probably because of the higher solubility of carbon in austenite and due to the lower diffusion rate. The austenite in Fe-Cr formed during laser treatment was relatively stable; no ferrite or martensite was formed, which can be ascribed to the high carbon content[14] and the small cell size.[15]

The Fe-W steel revealed an increase in hardness in the heat-affected zone due to the transformation of austenite to martensite. Already nucleated during the first passage of the laser,[8,9] it grows during the tempering treatment. The austenite itself did not have enough time to grow through the complete cell after resolidification. In the area where the temperature rises above the austenitizing point, $\delta$-ferrite is transformed to austenite. Further away from the molten area, there is diffusion of carbon and formation of carbides. At higher velocities, the highest hardness was found in the area which became austenitized. In this case, no martensite was found directly after solidification in the molten and resolidified area, because here only $\delta$-ferrite was formed.

In Fe-C, the wear rate increased in the annealed region where the hardness was lower, as expected, although the results were difficult to interpret due to some oxidative wear. The wear behavior of Fe-W is rather contradictory to the behavior of Fe-C. The wear rate decreases by a factor of 4 in the zone where carbides are formed, and cell walls are diffused to broader, shallower zones. (It can be understood, because the large martensitic areas behave as nucleation points for microcracking, whereas the fine distribution of carbides in a matrix with a higher tungsten content is less prone to fatigue,[16] which process can be compared to some extent with this wear equipment.)

## VI. CONCLUSIONS

1. Near the melted and resolidified area in Fe-W and Fe-C, martensite is formed.
2. In all areas, substantial diffusion occurs.
3. The redistribution of carbon and other alloying elements causes a precipitation of carbides in the interior of ferritic/martensitic cells.
4. No transformation was found in steel which was fully austenitic after the first laser treatment.
5. The martensitic areas in the heat-affected zones were harder than in the molten and resolidified zones; the zone with the carbides had a lower hardness.
6. A decrease of wear rate was found in the softer precipitated zones in Fe-W contradictory to the results in Fe-C where the softer annealed regions revealed a higher wear rate.
7. Besides some diffusion, no annealing effects were found in the austenitic Fe-Cr.

## ACKNOWLEDGMENTS

This work is part of the research program of the Foundation for Fundamental Research on Matter (FOM–Utrecht) and has been made possible by financial support from the Netherlands Organization for Research (NWO–The Hague).

## REFERENCES

1. Y.-W. Kim, P.R. Strutt, and H. Nowotny: *Metall. Trans. A*, 1979, vol. 10A, pp. 881-86.
2. P.R. Strutt, H. Nowotny, M. Tuli, and B.H. Kear: *Mater. Sci. Eng.*, 1978, vol. 36, pp. 217-22.
3. P.A. Molian and W.E. Wood: *Scripta Metall.*, 1982, vol. 16, pp. 1301-03.
4. P.A. Molian: *J. Mater. Sci.*, 1985, vol. 20, pp. 2903-12.
5. M. Riabkina-Fishman and J. Zahavi: *J. Mater. Sci.*, 1988, vol. 23, pp. 1547-52.
6. J. Kusinski: *Metall. Trans. A*, 1988, vol. 19A, pp. 377-82.
7. M.F. Ashby and K.E. Easterling: *Acta Metall.*, 1984, vol. 32, pp. 1935-48.
8. J.J. Rayment and B. Cantor: *Metall. Trans. A*, 1981, vol. 12A, pp. 1557-68.
9. S. Kou, D.K. Sun, and Y.P. Le: *Metall. Trans. A*, 1983, vol. 14A, pp. 643-53.
10. L. Åhman: *Metall. Trans. A*, 1984, vol. 15A, pp. 1829-35.
11. H. De Beurs and J.Th.M. De Hosson: *Scripta Metall.*, 1987, vol. 21, pp. 627-32.
12. H.J. Hegge and J.Th.M. De Hosson: Proc. 2nd Europ. Conf. Laser Treatments Mat., Bad Nauheim 13–14, Oct. 1988, DVS-Verlag GmbH, Düsseldorf 1988, pp. 160-63.
13. M.R. James, D.S. Gnanamuthu, and R.J. Moores: *Scripta Metall.*, 1984, vol. 18, pp. 357-61.
14. T. Minemura, A. Inoue, Y. Kojima, and T. Masumoto: *Metall. Trans. A*, 1980, vol. 11A, pp. 671-73.
15. Z. Nishiyama: *Martensitic Transformation*, Academic Press, New York, NY, 1978, pp. 280-92.
16. J.W. Martin: *Micromechanisms in Particle-Hardened Alloys*, Cambridge University Press, Cambridge, England, 1980, pp. 138-51.
17. W.C. Oliver, R. Hutchings, and J.B. Pethica: *Metall. Trans. A*, 1984, vol. 15A, pp. 2221-29.

18. G.R. Speich and W.C. Leslie: *Metall. Trans.*, 1972, vol. 3, pp. 1043-54.
19. S. Hertzman: *Metall. Trans. A*, 1987, vol. 18A, pp. 1753-66.
20. S. Björklund, L.F. Donaghey, and M. Hillert: *Acta Metall.*, 1972, vol. 20, pp. 867-74.
21. Y.L. Tien and R. W. Kraft: *Metall. Trans. A*, 1987, vol. 18A, pp. 1403-14.
22. E.J. Mittemeijer, L. Cheng, P.J. van der Schaaf, C.M. Brakman, and B.M. Korevaar: *Metall. Trans. A*, 1988, vol. 19A, pp. 925-32.